materials

MDPI

Article

Fused Filament Fabrication of Soda-Lime Glass Feedstocks

Thomas Hanemann [1,2,*], Hannes Hering [1], Martin Zürn [1,2], Ralf Eickhoff [1] and Dorit Nötzel [1]

[1] Institute for Applied Materials, Karlsruhe Institute of Technology, Hermann-von-Helmholtz-Platz 1, 76344 Eggenstein-Leopoldshafen, Germany
[2] Department of Microsystems Engineering, University of Freiburg, Georges-Köhler-Allee 102, 79110 Freiburg, Germany
* Correspondence: thomas.hanemann@kit.edu

Highlights

What are the main findings?

- Successful development of new soda-lime glass containing feedstocks suitable for fused filament fabrication.
- Feasibility of fused filament fabrication of small parts demonstrated.
- Dense small glass parts after debinding and sintering obtained.

What are the implications of the main findings?

- Feedstocks containing commercial soda-lime glass can be used for the realization of small dense glass parts by fused filament fabrication and thermal post-processing.

Abstract

Additive manufacturing methods are rather seldom used for the fabrication of glass parts. In this work, the knowledge gained from glass injection molding and ceramic fused filament fabrication (FFF) was extended to the usage of the FFF process chain covering the individual process steps compounding, 3D printing and thermal post-processing for the realization of soda-lime glass parts. The selection of suitable feedstock compositions, containing a soda-lime glass filler and a binder system, consisting of polyethylene glycol (PEG), polyvinyl butyral (PVB), and stearic acid (SA) is essential for successful processing. Small cuboid and disk-shaped parts could be first printed and second debound and sintered to parts with relative densities between 94 up 98% depending on the initial feedstock composition. A further extension to the printing of a larger-sized micro reactor possessing internal hollow structures showed the principal feasibility of soda-lime glass FFF printing. Due to the presence of defects after printing, debinding and sintering was omitted. Consequently, further material and process optimization is necessary to eliminate part distortion and other defects, which is mandatory prior to successful process chain evaluation.

Keywords: soda-lime glass; fused filament fabrication; FFF; PEG/PVB-based binder

Academic Editor: Yunping Li

Received: 26 October 2026
Revised: 9 November 2026
Accepted: 12 November 2026
Published: 16 November 2026

Copyright: © 2026 by the authors. Licensee MDPI, Basel, Switzerland. This article is an open access article distributed under the terms and conditions of the Creative Commons Attribution (CC BY) license.

1. Introduction

The manufacturing of polymers, metals, and ceramics is well established through melt-processing technologies, including various injection molding techniques for polymers and powder injection molding (PIM) for metals and ceramics [1,2]. In contrast, glass components are predominantly produced from the molten state at elevated temperatures, resulting in high energy consumption and considerable CO_2 emissions [3,4]. Moreover,

the fabrication of geometrically complex glass components remains challenging when using conventional glass-forming technologies. In this context, the well-established powder-processing routes employed for metals and ceramics offer a promising alternative for glass manufacturing [5].

This concept was successfully demonstrated by Zürn et al., who introduced the process referred to as glass injection molding (GIM) using borosilicate and soda-lime glass powders [6,7]. The GIM process chain comprises the following steps:

- Compounding;
- Injection molding;
- Debinding and sintering.

With regard to more sustainable processing, binder systems containing potentially bio-derived components, such as low-molecular-weight polyethylene glycol (PEG), have been developed for metal injection molding (MIM) and ceramic injection molding (CIM) [8]. PEG can be removed during aqueous pre-debinding and is often combined with a high-molecular-weight backbone polymer like poly(vinyl butyral) (PVB) and poly(methyl methacrylate) (PMMA) in combination with stearic acid (SA) or related fatty acids as surfactants. This binder concept was subsequently adapted for GIM applications [6,7]. By applying the GIM process chain described above, dense glass components based on borosilicate and soda-lime glass could be produced, achieving relative densities close to 100% of the theoretical density in both cases. For both material systems, extensive investigations of feedstock compositions and processing parameters were required to obtain defect-free, highly dense components. Further reviews and overviews of powder injection molding technologies incorporating glass powders as feedstock materials can be found in [9–11].

The most important additive manufacturing technologies, such as stereolithography (SLA) and fused filament fabrication (FFF), the latter belonging to the material extrusion (MEX) family, were developed during the final decades of the twentieth century primarily for the fabrication of polymer components [12]. Both technologies also enable the processing of composite materials by incorporating fillers such as carbon, natural, metal, or glass fibers, as well as carbon nanotubes and graphene, thereby allowing the production of polymer matrix composites (PMCs) [13].

In the case of SLA, dedicated material developments, particularly in the field of photocurable ceramic suspensions, have enabled the manufacturing of ceramic components [14,15]. The fabrication of ceramic parts by FFF has greatly benefitted from the extensive knowledge gained in ceramic injection molding (CIM), owing to the strong similarities between the respective process chains [16]. A comparable development has been observed for the additive manufacturing of metal parts [17]. In the literature, these FFF-based approaches are commonly denoted as ceramic fused filament fabrication (CF^3) and metal fused filament fabrication (MF^3), respectively [18,19].

Additive manufacturing of glass components is rather seldom described in the literature. In an analogous MEX approach, a soda-lime glass filament was melted by a CO_2 laser and deposited on a printing stage [20]. In a short overview Schilm et al. described two methods, CerAM T3DP, which is a variant of MEX, and CerAM VPP as a derivative of Stereolithography (SLA) [21]. In both cases, the processing of the Schott borosilicate glass 8250 was reported. In a more comprehensive review by Zhang et al. the state of the art in 2020 covering FFF and its variants, the family of SLA types, Selective Laser Sintering or Melting, and Direct Ink Writing [22] was reported. With respect to the fabrication of very fine structural features, the processing of silica nanocomposites by SLA delivered very precise and highly transparent silica parts [23]. Recent work described SLA of bioactive glass for potential usage in bone repair [24] and the introduction of volumetric additive manufacturing methods [25]. FFF printed bioactive glass-ceramic systems were used for scaffold realization [26].

https://doi.org/10.3390/ma19224853

Despite the vicinity of injection molding and FFF, especially in case of highly filled feedstocks for the generation of ceramic, metal or glass parts, a direct one-to-one adaption is not possible. This can be attributed to strong process distinctions. Injection molding is a high-pressure technology, where the feedstock melt is injected into the molding tool under high pressure and injection speed. The latter corresponds with huge shear rates up to 3500 1/s during injection. FFF can be treated as almost pressure-less method and slow filament conveying speed equivalent to small shear rates in the range of 50 to 100 1/s. Highly filled feedstocks show a pronounced shear-thinning flow behavior, which hampers FFF printing. Under identical conditions, FFF faces a higher feedstock viscosity than injection molding. Therefore, the feedstock's melt viscosity is a very critical issue. In principle, a viscosity reduction can be achieved by increasing the temperature. However, this may have a negative impact on other printing parameters. Furthermore, the feedstock composition can be altered by thermal decomposition. To ensure that the FFF process window remains stable, the melting viscosity must be lower than that of PIM when the same solid load is used. One established solution is the usage of suitable additives like plasticizers and surfactants and the variation in their concentration in the used binder system, as developed, e.g., for powder injection molding [27]. Fatty acids are established surfactants in PIM and FFF, especially stearic acid (SA) is often used [27–29]. A SA content increase normally causes a viscosity drop at constant temperature up to a factor of 10 [30].

This work focuses on the establishment of FFF for the realization of glass components made of soda-lime glass. Previous investigations on injection molding of soda-lime glass applying a binder combination of PEG, PVB in combination with SA as surfactant were used as starting point [7]. Under consideration of the above-mentioned viscosity issues, the focus was set on the impact of different SA amounts on compounding, achievable maximum filler load, melt viscosity, printing and final part quality.

2. Materials and Methods

2.1. Material Selection

Details of the as filler used commercial soda-lime glass Swarcoforce from Swarco Indusferica (Neufurth, Austria), were reported in [7,31]. To sum up, the most relevant filler properties are:

- Spherical particle morphology;
- Particle size distribution: d_{10}: 2.9 µm, d_{50}: 6.1 µm, and d_{90}: 9.9 µm;
- Specific surface area 0.78 m^2/g;
- Density of 2.5 g/cm^3 as supplied by the vendor [31].

As in previous work dealing with GIM of borosilicate or soda-lime glass as well as FFF of different ceramic or metal fillers, PEG as a water-soluble low-molecular-weight binder component, PVB as a high-molecular-weight binder component, and SA as a surfactant were used [6,7,18,19]. Table 1 lists all investigated binder components and their functionality. With the listed materials new soda-lime glass-based feedstocks with respect to their usability in FFF were developed. The solid glass filler load was initially set to 55 Vol%, the ratio of the two main binder components—PEG and PVB—was varied. in accordance with Weber [8], the amount of SA was compensated by an equivalent reduction in the PVB backbone polymer moiety. While the same PVB type was used, two different PEGs were selected to validate the impact of the PEG's average molecular mass on subsequent processing.

Table 1. Used binder components, their functions, and the related suppliers.

Binder Component	Function	Supplier
PEG 8000	Plasticizer	Carl Roth GmbH + Co. KG, Karlsruhe, Germany

PEG 20,000	Plasticizer	Carl Roth GmbH + Co. KG, Karlsruhe, Germany
PVB B30H	Backbone Polymer	Kuraray Europe GmbH, Hattersheim a. M., Germany
SA	Surfactant	Carl Roth GmbH + Co. KG, Karlsruhe, Germany

2.2. Compounding and Rheological Characterization

All newly developed feedstocks were compounded using a torque-measuring mixer (W50 EHT, Brabender, Duisburg, Germany), enabling continuous monitoring of the mixing torque throughout the process. Compounding was carried out at 125 °C for 1 h at a rotational speed of 30 rpm in a 50 cm^3 mixing chamber. For all mixtures three individual measurements were conducted. The individual error of one data point within one measurement is ± 0.5 Nm. Following compounding, the rheological behavior of the feedstocks was analyzed using a high-pressure capillary rheometer (Rheograph 25, Göttfert GmbH, Buchen, Germany) equipped with a capillary of 30 mm length and 1 mm diameter. Measurements were conducted three times at 140 °C over a shear rate range of 1 to 3500 s^{-1}. The obtained melt viscosities were subsequently corrected using the Weißenberg-Rabinowitsch method [32].

2.3. Filament Extrusion

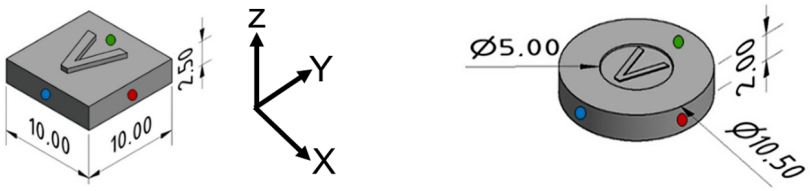
Filaments prepared out of the different feedstock systems were extruded by a single-screw filament extruder (Noztek Pro, Noztek, Shoreham-by-Sea, UK) equipped with a 2.85 mm nozzle. The extruders extrusion speed was set by the vendor to a fixed value of 50 rpm. The hot extruded strands were cooled using a home-made alumina cooling track in air. The filament diameter was measured via a micrometer caliper under ambient conditions. The experimental error is in the rage of ±0.05 mm.

2.4. FFF Printing

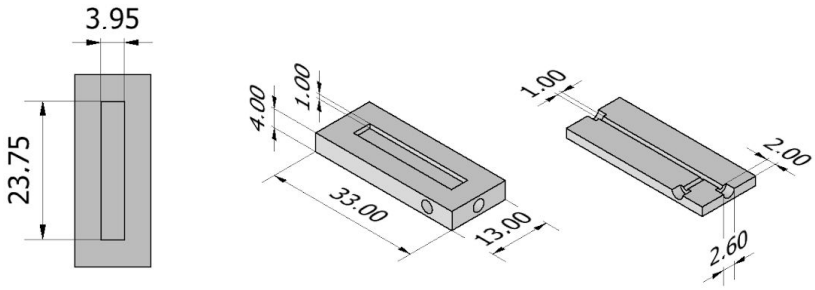
A German RepRap x350 pro (German RepRap GmbH, Feldkirchen, Germany) MEX printer was applied for part printing. The print head was replaced by a Titan Extruder (E3D, Oxfordshire, UK). To prevent annular backflow due to insufficient filament cooling, the modified printhead was additionally equipped with two cooling fan push-pull cooling system enabling a continuous air flow. The specimens were printed on a polyethylene covered spring steel plate. Ultimaker Cura 5.4 was applied as a slicer for the generation of the G-code files. The relevant printing parameters can be found in Section 3.4.

2.5. Test Structures

Two different small test parts (cuboid, disk) were selected to show the principal feasibility of FFF printing (Figure 1a,b). The colored dots represent the positions for geometry measurements. In addition, a microreactor design, as described in [7], has been selected as more complex and larger part containing hollow structures inside (Figure 1c).



(**a**) (**b**)



(**c**)

Figure 1. Test structures (sizes in mm): (**a**) Cuboid; (**b**) Disk; (**c**) Micro reactor test design with hollow structures inside.

2.6. Injection Molding

To provide a reference for comparison, disk-shaped components measuring 10.5 mm in diameter and 2 mm in thickness were produced via micro injection molding, following the approach reported earlier [7]. The fabricated geometry corresponded to the specimen illustrated in Figure 1b, excluding the "V"-shaped structure. Molding experiments were conducted on a Microsystem 50 machine (Battenfeld, Kottingbrunn, Austria) using mold inserts manufactured from tool steel. Process parameters were selected according to those reported in [7].

2.7. Debinding and Sintering

All printed and injection-molded samples were debound in two steps. First, the green-bodies were pre-debound in a water bath for at least 16 h at 40 °C for accelerated PEG dissolution [7,8] followed by sample drying at 50 to 80 °C. Second, thermal debinding was performed in a chamber oven HT/28 (Carbolite Gero, Neuhausen, Germany) with a maximum temperature of 550 °C. Details can be found in Table 2. Finally, sintering followed in a Carbolite Gero RHF 1700/5 furnace (Neuhausen, Germany) with a maximum temperature of 670 °C under air atmosphere (Table 3).

Table 2. Temperature program for thermal debinding.

Step	Temperature Range (°C)	Heating Rate (°C/min)	Dwell Time (min)
1	25–120	3	-
2	120–220	0.2	-
3	220	-	60
4	220–330	0.1	-
5	330	-	300
6	330–550	0.2	-
7	550	-	120
8	550–25	3	-

Table 3. Applied sinter program.

Step	Temperature Range (°C)	Heating/Cooling Rate (°C/min)	Dwell Time (min)
1	25–330	3	-
2	330–550	0.5	-
3	550	-	60
4	550–670	0.5	-
5	670	-	240
6	670–25	3	-

2.8. Sintered Glass Part Characterization

The sintered density of all additively manufactured soda-lime glass parts was evaluated according to Archimedes' principle using water as the displacement medium and a YDK01 balance (Sartorius, Göttingen, Germany). A detailed description of the methodology can be found in [7]. Dimensional shrinkage after sintering was determined from measurements taken at the indicated locations in Figure 1a,b using a VRZ1 incremental length measurement system (J. Heidenhain GmbH, Traunreut, Germany). In addition, selected specimens were examined by computed tomography (Phoenix v|tome|xs, General Electric, Frankfurt, Germany) to identify internal flaws, including voids and cracks. Imaging was conducted at a spatial resolution of 15 µm with a measuring time of 100 ms, operating at 100 kV and 120 µA.

3. Results and Discussion

3.1. Feedstock Compounding

As a result of preliminary investigations five different feedstocks were selected for process chain evaluation (Table 4). To meet the requirements of a low melt viscosity for FFF printing, the impact of the SA content increase, accompanied with a simultaneous PVB decrease, on compounding and further processing was investigated. The denomination of the feedstocks follows the Swarcoforce filler load (initial SF55 or extended to SF60), the **s**tearic acid content (SA35, SA60, SA90) and the special usage of PEG 8000 (PEG8K) instead of PEG 20,000. The compositions were selected to investigate the surfactant concentration, the average molecular PEG mass as well as the influence of the solid load on the processing behavior like rheology, printing, and final part properties like density. By experience [6–8,18,19] it was advantageous, to retain an identical sequence of the different binder component addition into the mixing chamber. First, a small portion of the glass filler was given into the chamber until complete coverage of the dough hooks, followed by a complete addition of all organic moieties and concluded with the remaining glass powder. Figure 2a shows the measured torque with compounding time at 125 °C [7]. The compounding process can be subdivided into three stages:

- Filling state: All materials were added to mixing chamber;
- Mixing state: Start of glass filler wetting by surfactant and binder;
- Stationary state: Equilibrium between surfactant adsorption and desorption.

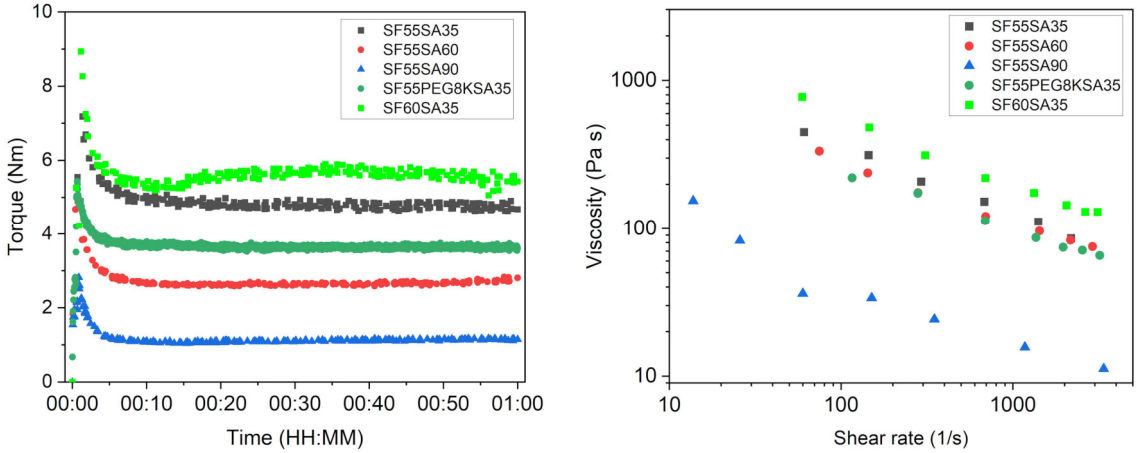
At constant solid load the equilibrium torque drops with increasing SA concentration from 4.7 Nm to 1.1 Nm. For the sake of completeness, it must be mentioned that a SA content increase corresponds with a PVB content decrease. Hence the observed torque drop has its origins in both—SA and PVB—concentration changes. The substitution of PEG 20,000 with PEG 8000 at constant solid load and SA concentration lead to a torque drop as well. An increase in the solid load from 55 Vol% to 60 Vol% caused only a small equilibrium torque elevation from 4.7 Nm to 5.4 Nm. Previously reported investigations showed that feedstocks with PEG 8000 instead of PEG 20,000 delivered a lower equilibrium torque at 55 Vol% as well as 60 Vol%, respectively (4.9 Nm down to 3.7 Nm and 5.6 Nm down to 3.9 Nm) [7].

Table 4. Feedstock compositions investigated.

Denomination	Solid Load (Vol%)	PEG (Vol%)	PVB (Vol%)	Surfactant SA (mg/m²)	Surfactant SA (Vol%)
SF55SA35 [(a)]	55	22.5 [a]	18.6	35	3.9
SF55SA60 [(a)]	55	22.5 [a]	15.8	60	6.7
SF55SA90 [(a)]	55	22.5 [a]	12.5	90	10.0

SF55PEG8KSA35 [(b)]	55	22.5 [b]	18.6	35	3.9
SF60SA35 [(a)]	60	20.0 [a]	15.7	35	4.3

[(a)] PEG 20,000; [(b)] PEG 8000.



(**a**) (**b**)

Figure 2. Characterization of all investigated feedstocks: (**a**) Compounding at 125 °C, (**b**) Shear rate dependent melt viscosity at 140 °C.

3.2. Melt Viscosity

For both relevant polymer melt-processing replication techniques—IM for mass fabrication and FFF for rapid prototyping—a clear determination of the shear rate dependent viscosity is mandatory. Figure 2b presents the viscosity dependence with feedstock composition and shear rate. At a constant solid load of 55 Vol%, the SA rise from 35 to 60 mg/m² caused a small viscosity drop, the additional increase to 90 mg/m² yielded a further drop by a factor of 10. The substitution of PEG 20,000 by PEG 8000 at a SA content of 35 mg/m² lead only to a small viscosity reduction. An increase in filler load from 55 Vol% to 60 Vol% lead to a moderate viscosity rise.

While in IM shear rates up to several thousand can occur, in FFF typical shear rates, depending on the used nozzle diameter, nozzle previous printed layer gap and filament feeding speed, between 50 and 100 1/s can be assumed. Table 5 summarizes the relevant data obtained from compounding and melt viscosity measurements, including equilibrium torque, estimated viscosity values at 100 1/s and 1000 1/s, and the ratio of the latter ones. At constant solid load of 55 Vol% a SA-increase from 35 to 90 mg/m² caused in all cases a drop of the equilibrium torque and viscosity values as well as of the calculated viscosity ratio from 3.3 down to 2.3. This can be interpreted as a reduction in the polymer chain de-entanglement impact on the shear thinning flow and a strong influence of the huge amount of SA. It has to be mentioned that the SA-content increase correlates with a PVB content decay. The substitution of PEG 20,000 by PEG 8000 delivered a moderate viscosity drop over the whole shear rate range and of the viscosity ratio as well, which can be explained by the shorter polymer chains and the reduced chain entanglement. A higher solid filler load shifts the viscosity values and the viscosity ratio to higher values, which agrees to earlier investigations [7]. In [7] the ratio of PEG and PVB was 1:1, here the PEG content is always higher than the PVB moiety. Therefore, systems with identical solid load and SA content possess lower viscosity values at an identical measuring temperature.

Table 5. Overview of the equilibrium torque after 1 h at 125 °C, melt viscosity (140 °C) at two different shear rates typical for FFF (100 1/s) and injection molding (1000 1/s) as well as the derived viscosity ratio.

Feedstock	Equilibrium Torque (Nm)	Estimated Viscosity @100 1/s (Pa s)	Estimated Viscosity @1000 1/s (Pa s)	Viscosity Ratio
SF55SA35	4.7 ± 0.7 [a]	350	105	3.3
SF55SA60	2.8 ± 0.5 [a]	300	100	3.0
SF55SA90	1.1 ± 0.4 [a]	35	15	2.3
SF55PEG8KSA35	3.6 ± 0.7 [a]	200	100	2.0
SF60SA35	5.4 ± 1.2 [a]	600	200	3.0

[a] Equilibrium torque value and standard deviation.

3.3. Filament Extrusion

For successful FFF printing the used filament must fulfill certain geometrical (constant diameter) and physical (certain stiff- and hardness) requirements, which are relevant for continuous filament conveying by the gear wheels. First, the diameter deviation should be as small as possible and second, the surface should be very smooth without any remarkable surface roughness or steps. To achieve this, test trials delivered for the selected feedstock systems optimized extrusion temperatures and filament diameters (Table 6). All filaments were not flexible. After filament cooling on the metal track, the strands were cut in pieces with a length of 50 cm.

Table 6. Optimized filament extrusion temperature and measured filament diameter.

Feedstock	Extrusion Temperature (°C)	Obtained Filament Diameter (mm)
SF55SA35	150	2.8
SF55SA60	150	2.7
SF55SA90	140–165	2.7
SF55PEG8KSA35	145–155	2.7
SF60SA35	150	2.8

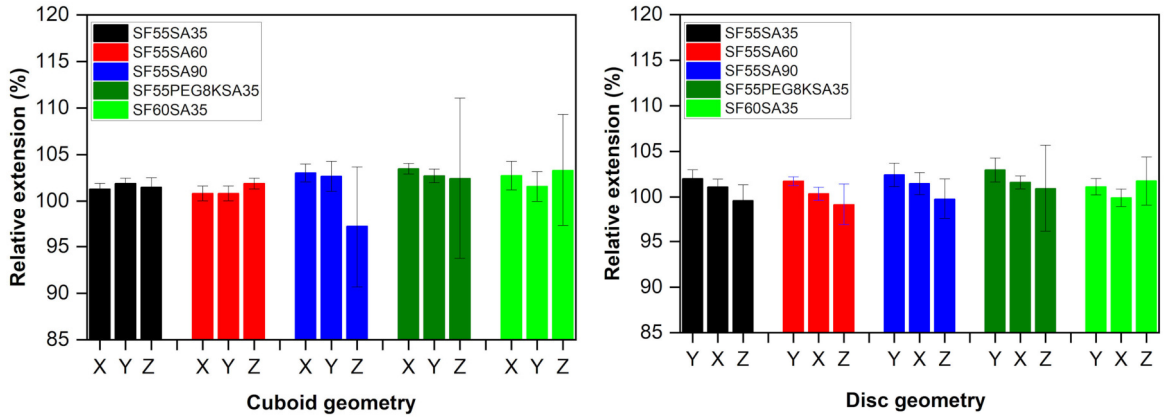
3.4. FFF Printing

Table 7 lists all used printing parameters optimized for each feedstock composition. The individual layer orientation was 0° and 90°, delivering the small parts as presented in Figure 1a,b. After printing, the green-body geometry (layer x,y, height z) of the cuboids and disks was measured to investigate the accuracy of the printing process itself (Figure 3). Six samples were considered for mean value and standard deviation calculation. In case of the cuboids, all measured extensions in x,y-direction were larger as the nominal value. With exception of the z-value of SF55SA90, this is also valid for the z-direction. Irrespective of the applied feedstock composition, all systems delivered similar results. In case of the disks, all systems show higher values for the x- than the y-direction. The z-value is even smaller than the others. For the feedstock with a solid load of 60 Vol%, no trend can be observed. The deviation between x,y and z-direction can be explained by the different types of positioning on the print bed. And even in x,y due to the different motor characteristics and positioning accuracy non-unique values can be expected.

Table 7. Optimized printing parameters.

Denomination	Printing Temperature (°C)	Nozzle Diameter (mm)	Layer Thickness (mm)	Infill (%)	Flow (%)	Printing Speed (mm/s)	Built Plate Temperature (°C)
SF55SA35	180	0.4	0.1	105	100	7.5	50

SF55SA60	180	0.4	0.1	100	100	10	60
SF55SA90	220	0.4	0.1	100	98	10	50
SF55PEG8KSA35	190	0.4	0.1	105	98	7.5	50
SF60SA35	200	0.4	0.1	105	98	7.5	50



(**a**) (**b**)

Figure 3. Relative extension to the nominal value of printed green bodies: (**a**) Cuboids; (**b**) Disks.

3.5. Debinding

In a continuation of previous work on IM molding of PEG/PVB feedstocks, liquid pre-debinding prior to thermal debinding to obtain defect-free parts is essential [7]. It was demonstrated that the selection of suitable parameters allowed for a complete removal of all water-soluble binder moieties, here mostly PEG [6]. Table 8 lists for the cuboids (6 samples), the disks (6 samples), and for comparison, the used filament (4 samples), the average percentage of all water-soluble binder moieties loss for all investigated feedstocks.

Table 8. Comparison of relative mass loss during water debinding for all used part geometries plus filament as reference.

	Relative Mass Removal Related to PEG Content (%)		
Denomination	**Cuboid**	**Disks**	**Filament**
SF55SA35	99.0 ± 0.3	99.9 ± 0.4	101.3 ± 1.4
SF55SA60	99.3 ± 1.5	99.9 ± 0.4	100.0 ± 0.7
SF55SA90	99.4 ± 0.2	99.7 ± 0.4	99.9 ± 0.1
SF55PEG8KSA35	98.5 ± 0.4	99.4 ± 0.4	100.0 ± 0.1
SF60SA35	98.9 ± 0.4	99.5 ± 0.3	100.1 ± 0.1

In all cases, the removal rate is in the range between 98.5 and 100%, which is a very good result and can be attributed to the small sample thickness equivalent with short diffusion paths. Some of the filaments show a removal larger than 100% related to the initial PEG content; this can be attributed to the high SA content and was reported earlier as well [6]. After the pre-debinding step, thermal debinding followed (Table 2) enabling a complete PVB removal.

3.6. Sintering

After debinding, all samples were sintered applying the sinter program shown in Table 3 with a maximum sinter temperature of 670 °C according to [7] being a compromise between best sinter density and reduced geometric precision. Table 9 lists for the cuboids, the disks as well as the filament all obtained density values. As reference value the density supported by the vendor of 2.5 g/cm^3 was applied. In case of the cuboids (6 samples) and

the disks (6 samples), the SA-content increase from 35 to 90 mg/m² caused a slight average density increase. The higher solid load did not show a remarkable higher sinter density. For both specimen types the use of the lower molecular mass PEG 8000 lead to a lower density. The average sinter densities of the different filaments (4 samples) were all close to 100% th. The cuboids possess slightly higher density values than the disks. The filament densities are, in general, slightly higher than the related values for the FFF printed specimens. This may be attributed to the generation of small voids during printing yielding a reduced sinter density of the printed samples. Similar density values around 99–100% th. were obtained for injection-molded samples described in [7] using feedstock compositions with PEG 20,000 as binder component and solid loadings of 55 Vol% and 60 Vol%, respectively.

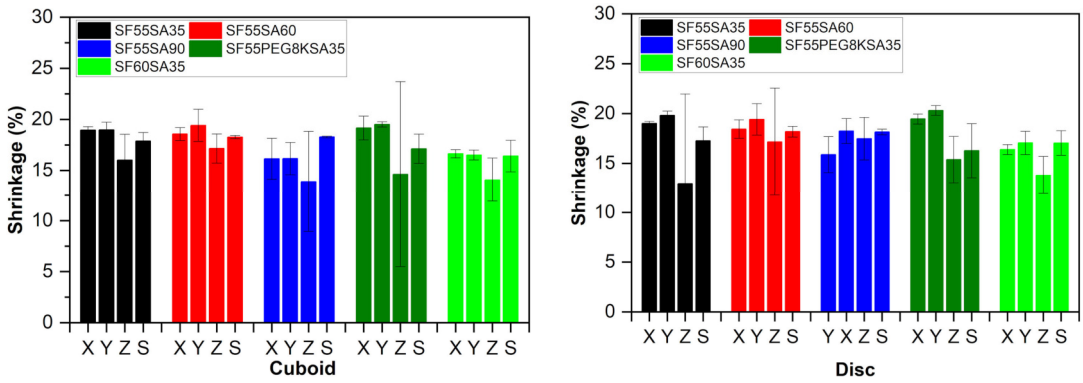
Table 9. Comparison of all measured density values.

	Densities (% th.)		
Denomination	**Cuboids**	**Disks**	**Filament**
SF55SA35	97.0 ± 3.0	94.9 ± 4.7	98.4 ± 0.1
SF55SA60	98.2 ± 0.6	98.0 ± 1.9	98.0 ± 1.3
SF55SA90	98.3 ± 0.3	97.9 ± 1.1	98.0 ± 0.9
SF55PEG8KSA35	94.3 ± 4.9	91.9 ± 8.7	98.0 ± 0.7
SF60SA35	97.4 ± 1.7	96.8 ± 3.1	98.8 ± 0.1

Under consideration of an isotropic sinter shrinkage, a simple correlation between the nominal linear shrinkage S_L with the measured green-body D_G and sinter densities D_S can be derived [33] (1):

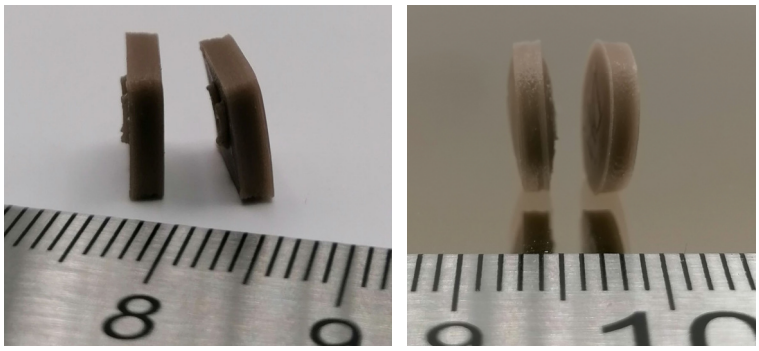
$$S_L = 1 - \sqrt[3]{\frac{D_G}{D_S}} \approx 1 - \sqrt[3]{\phi} \quad (1)$$

The ratio of the theoretical green-body density to the theoretical sinter density corresponds to the relative solid loading (ϕ). The solid loadings investigated were 0.55 (eq. 55 Vol%) or 0.60 (eq. 60. Vol%) and come along with theoretical linear shrinkage values of 18.1% or 15.7%, respectively. Figure 4a (cuboid) and Figure 4b (disk) show the comparison of the measured x,y,z-linear shrinkage with the nominal value S. In both cases, a deviation of the nominal value with the measured ones can be seen. A systematic correlation between pristine feedstock composition and shrinkage cannot be observed. Only the higher solid load in the SF60SA35 system causes a slightly lower shrinkage value. The shrinkage in z-direction is in almost all cases smaller than in x,y-direction and the nominal value. Possible explanations can be a non-isotropic shrinkage and technical challenges during the x,y,z-extension measurements. But in general, the measured shrinkage values fit to the nominal shrinkage value in an acceptable manner. Figure 5 shows exemplary for some sintered cuboids and disks a pronounced warpage and swelling. Figure 6a shows the CT scan of a disk as well as a cuboid made from SF55SA60. Some minor defects at the surface and in the bulk can be detected, but the measured sinter density around 98% th. seems to be realistic. In contrast, Figure 6b shows the identical parts but made from SF55PEG8KSA35. An extreme blowing up and a lot of defects especially in the bulk can be observed and explains the poor sinter density around 92% th. as well as the broad standard deviation. Under consideration of the CT-images, the measured density values according to the Archimedes method should be interpreted carefully, because only closed porosity is included. The defects shown belong to a certain extent, e.g., size, to open porosity and can falsify the measured density.



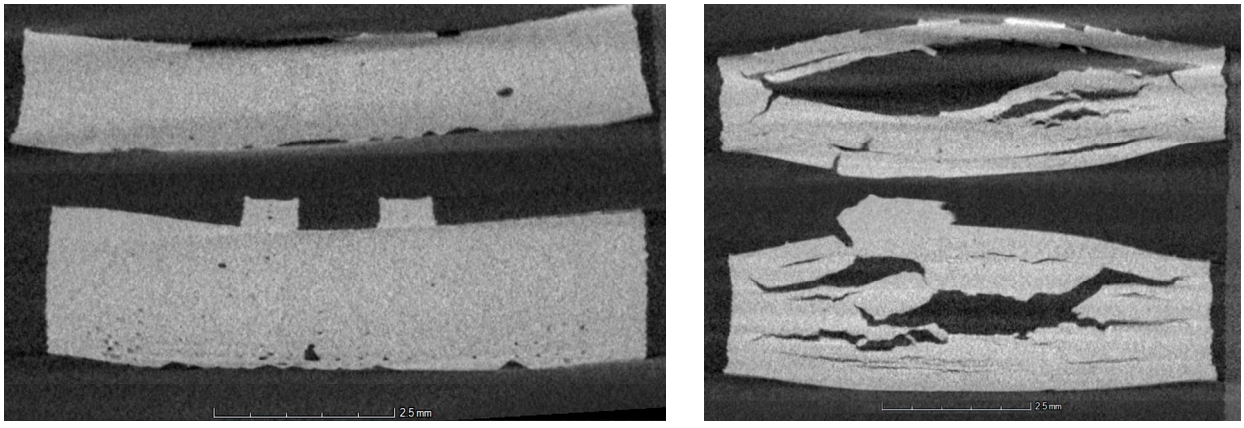
(**a**) (**b**)

Figure 4. Sinter shrinkage: (**a**) Cuboids; (**b**) Disks.



(**a**) (**b**)

Figure 5. Pronounced sinter warpage and swelling: (**a**) Cuboids (made from SF55SA60); (**b**) Disks (made from SF55PEG8KSA35).



(**a**) (**b**)

Figure 6. CT images of selected sintered samples. Upper sample disk, lower sample cuboid: (**a**) Samples made from SF55SA60; (**b**) Samples made from SF55PEG8KSA35.

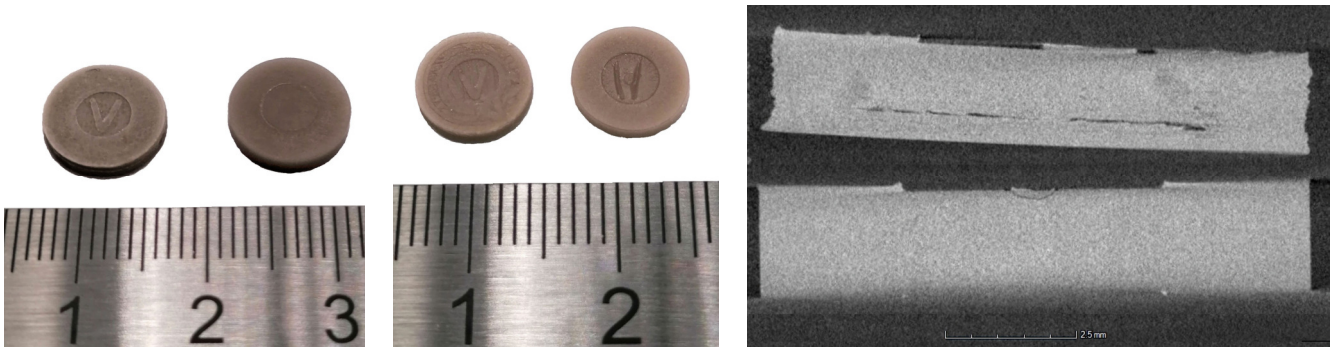
3.7. Injection Molding of SF55SA60

Due to the use of mold inserts and the injection of the polymer under high pressure, injection molding delivers dense parts in a reproducible and reliable quality. Comparing GIM with FFF, 6 disks each made from SF55SA60, possessing very good sinter bulk densities, were realized and further processed under identical conditions. Table 10 shows the obtained data. The standard deviations of the via GIM fabricated green body geometry are smaller than the FFF ones. Consequently, the same is valid for the sintered samples. Sintered samples made from a similar feedstock and processed by IM possessed a density

around 99.1 ± 1.6% th. [7]. Within the experimental errors the sinter densities of injection-molded and 3D printed samples are identical (Table 10). Figure 7a,b presents microscopic images of FFF and IM derived green bodies and sintered parts as well as one CT image. Especially the latter one shown in Figure 7c gives an impression about the part quality depending on the fabrication method. Whilst the GIM derived part (down) possesses a defect-free bulk appearance, the FFF printed part (up) shows a clear layer delamination in the bulk originating from the printing process and a poor layer-to-layer adhesion.

Table 10. Comparison of disks fabricated by IM and FFF applying feedstock SF55SA60.

	IM			FFF		
Axis	**x**	**y**	**z**	**x**	**y**	**z**
Green body Dimension (mm)	10.50 ± 0.01	10.49 ± 0.01	2.12 ± 0.01	10.67 ±0.05	10.51 ±0.10	2.04 ± 0.09
Sinter body Dimension (mm)	8.71 ± 0.05	8.74 ±0.1	1.73 ± 0.01	8.70 ± 0.16	8.53 ± 0.09	1.69 ±0.12
Density (% th.)		98.9 ± 0.1			98.0 ± 1.9	

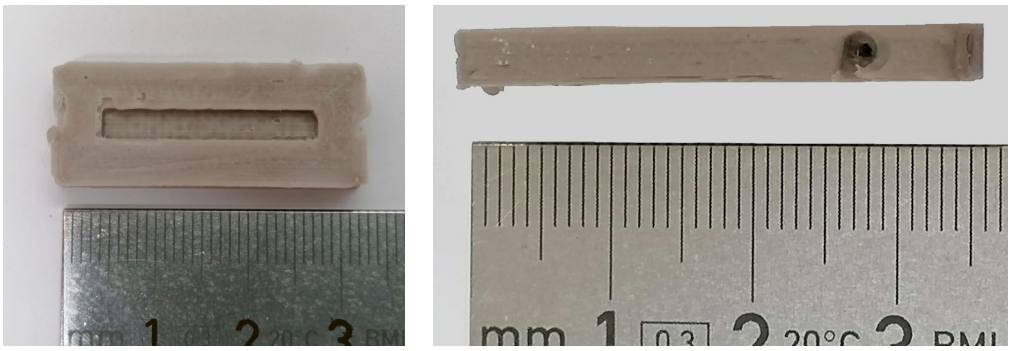


(**a**) (**b**) (**c**)

Figure 7. Comparison of FFF-printed and GIM fabricated parts ((**a**,**b**), **left**) and GIM ((**a**,**b**), **right**) fabricated disks: (**a**) Green bodies; (**b**) Sintered parts; (**c**) CT-images, up FFF-printed, down GIM.

3.8. FFF Printing of Larger Parts

Micro fluidic applications are besides of micro optics one of the most promising application fields for non-silicon micro components. Especially micro reaction technology possesses many interesting functional components like mixer or micro reactors. Injection molding was used to fabricate micro reactor shelfs made from, e.g., soda-lime glass [7]. As a drawback, this half shelfs must be sinter-joined after molding. In contrast, FFF enables the fabrication of the complete device without any post-processing like joining. Applying again feedstock SF55SA60, the micro reactor design presented in Figure 1c was selected for FFF printing trials (Figure 8). Especially at the corners of the device (Figure 8a) and in the vicinity of the fluid opening (Figure 8b) some structural defects can be seen. In general, overhangs are quite often a challenge to be realized defect-free. Unfortunately supporting structures cannot be used here to retain the channel open. Due to the presence of these surface defects further processing towards sintered parts was waived.



(a) **(b)**

Figure 8. Printed reactor test structure: (**a**) Top view; (**b**) Side view.

4. Conclusions

New feedstock systems were evaluated with respect to the usage in FFF towards the realization of dense glass parts. Along the whole process chain compounding, printing and thermal post-processing the most important findings are summarized in the following:

1. Soda-lime glass containing feedstocks with a solid load of 55 Vol% or 60 Vol% in combination with PEG/PVB binder systems and stearic acid as surfactant were realized and characterized in the molten state with respect to their rheological properties. The influence of the surfactant, the solid load and the PEG's average molar mass on the flow behavior was evaluated.
2. All selected feedstocks could be used in FFF printing of small parts successfully. With respect to processing and final sinter part characterization, the mixture SF55SA60 seems to be the most suitable composition.
3. The feedstock SF55SA60 was also successfully used in injection molding.
4. All relevant parameters for liquid pre-debinding and thermal debinding were evaluated successfully.
5. Sintering enabled for almost all feedstock systems the realization of small dense glass parts. However, part warpage and inflation were observed partially.
6. A first demonstrator device, here a small micro reactor with internal hollow structures, could be processed. After printing, pronounced surface defects could be observed. Therefore, debinding and sintering was omitted.

The principal feasibility of glass FFF applying PEG/PVB feedstocks was demonstrated. After sintering many of the small parts were warped or distorted. FFF printing of more complex parts with internal overhangs suffered from some reduced surface and geometric feature quality.

5. Outlook

Future work must concentrate on the improvement of the printed part quality and the realization of larger devices in a reliable quality with a focus on accuracy and mechanical stability without delamination issues. Possible approaches can be the increase in the solid load towards 60–65 Vol%, the use of the more rigid polymer PMMA instead of PVB in combination with the addition of a suitable plasticizer enabling a more flexible filament and an elimination of internal stress preventing warpage. The realization of complex glass structures with internal open channels and connections to peripheral equipment, such as chemical reaction plants, will only be possible if these challenges are successfully addressed. Same will be valid for the generation of fragile glass parts as shown by Hambitzer et al. [34].

Author Contributions: Conceptualization, M.Z. and T.H.; methodology, M.Z.; validation, M.Z., formal analysis, R.E., D.N. and M.Z.; investigation, H.H. M.Z., D.N. and R.E.; resources, T.H.; data curation, H.H., M.Z. and T.H.; writing—original draft preparation, T.H.; writing—review and editing, TH; visualization, M.Z. and TH; supervision, D.N. and T.H.; project administration, T.H.; funding acquisition, T.H. All authors have read and agreed to the published version of the manuscript.

Funding: This research was funded by the German Research Foundation (DFG) within the framework of the bilateral project HA1924/35-1 "Kontinuierliche Hydrothermalsynthese von magnetischen Ferritnanopartikeln: Reaktionsmonitoring und Anwendung in der Additiven Fertigung von Funktionsmaterialien".

Data Availability Statement: The original data presented in the study are openly available in KITOpen Repository https://doi.org/10.35097/j35g1z3wxbbjpf8v.

Acknowledgments: The authors thank Peter Holzer for performing the injection molding experiments and IAM-AWP for providing the CT-Device (Phoenix v|tome|xs, General Electric, Frankfurt, Germany).

Conflicts of Interest: The authors declare no conflicts of interest.

Abbreviations

The following abbreviations are used in this manuscript:

CIM	Ceramic Injection molding
CF^3	Ceramic Fused Filament Fabrication
FFF	Fused Filament Fabrication
GIM	Glass Injection Molding
IM	Injection Molding
MEX	Material Extrusion
MF^3	Metal Fused Filament Fabrication
MIM	Metal Injection Molding
PEG	Polyethylene Glycol
PIM	Powder Injection Molding
PMMA	Polymethylmethacrylate
PVB	Polyvinyl Butyral
SA	Stearic Acid
SF	Swarcoforce
SLA	Stereolithography
Vol%	Volume%

References

1. Czepiel, M.; Bankosz, M.; Sobczak-Kupiec, A. Advanced Injection Molding Methods: Review. *Materials* **2023**, *16*, 5802. https://doi.org/10.3390/ma16175802.
2. Momeni, V.; Hufnagl, M.; Shahroodi, Z.; Gonzalez-Gutierrez, J.; Schuschnigg, S.; Kukla, C.; Holzer, C. Research Progress on Low-Pressure Powder Injection Molding. *Materials* **2022**, *16*, 379. https://doi.org/10.3390/ma16010379.
3. Schmitz, A.; Kamin'ski, J.; Maria Scalet, B.; Soria, A. Energy consumption and CO_2 emissions of the European glass industry, *Energy Policy* **2011**, *39*, 142–155. https://doi.org/10.1016/j.enpol.2010.09.022.
4. Butler, J.H.; Hooper, P.D. Chapter 15—Glass Waste. In *Waste*; Letcher, T.M., Vallero, D.A., Eds.; Academic Press: London, UK, 2019; pp. 307–322. https://doi.org/10.1016/B978-0-12-815060-3.00015-3.
5. Glass Melting and Hot Forming. Available online: https://www.schott.com/en-gb/expertise/glass-melting-and-hot-forming (accessed on 12 December 2025).
6. Zuern, M.; Schrage, A.; Antusch, S.; Bohn, N.; Holzer, P., Hanemann, T. Development of a Polyethylene Glycol/Polymethyl Methacrylate-Based Binder System for a Borosilicate Glass Filler Suitable for Injection Molding. *Materials* **2024**, *17*, 1396. https://doi.org/10.3390/ma17061396.

7. Zuern, M.; Antusch, S.; Noetzel, D.; Schrage, A.; Walter, H.; Hanemann, T. Development of a Soda-Lime Glass Feedstock for Injection Molding. *Materials* **2026**, *19*, 854. https://doi.org/10.3390/ma19050854.
8. Weber, O. Wasserlösliche Bindersysteme zum Minimieren von Pulver-Binder-Segregationseffekten im Mikropulverspritzguss. Ph.D. Dissertation, Albert-Ludwigs-Universität Freiburg im Breisgau, Freiburg im Breisgau, Germany, 2015. https://doi.org/10.6094/UNIFR/10149. (In German)
9. Moritz, T.; Schilm, J.; Mannschatz, A.; Peschel, M. Glass Powder Injection Molding—Ceramic Processing Applied to Glass Components. *Ceram. Appl.* **2014**, *2*, 44–49.
10. German, R.M.; Hens, K.F.; Lin, S.-T.P. Key Issues in Powder Injection Molding. *Ceram. Bull.* **1991**, *70*, 1294–1302.
11. Bose, A. Prof Randall M German: Shaping the field of Powder Injection Moulding—A MIM2025 tribute. *Powder Inject. Molding Int.* **2025**, *19*, 97–129.
12. Islam, A.; Mobarak, H.; Rimon, I.H.; Al Mahmud, Z.; Ghosh, J.; Ahmed, M.S.; Hossain, N. Additive manufacturing in polymer research: Advances, synthesis, and applications. *Polym. Test* **2024**, *132*, 108364. https://doi.org/10.1016/j.polymertesting.2024.108364.
13. Rahman, M.M.; Islam, S.; Mubasshira; Islam, M.S.; Ahammad, R.; Islam, M.A.; Hasib, M.A.; Rahman, M.S.; Moshwan, R.; Ehsan, M.M.; Rabbi, M.S.; et al. Polymer Composites in Additive Manufacturing: Current Technologies, Applications, and Emerging Trends. *Polymers* **2026**, *18*, 192. https://doi.org/10.3390/polym18020192.
14. Chen, J.-Y. Advances in ceramic 3D printing technologies and optimization research. *Int. J. Adv. Manuf. Technol.* **2025**, *140*, 2341–2376. https://doi.org/10.1007/s00170-025-16380-3.
15. Materialize Your Vision. Available online: https://www.lithoz.com/en/materials/materialoverview/ (accessed on 2 November 2026).
16. Spina, R.; Morfini, L. Material Extrusion Additive Manufacturing of Ceramics: A Review on Filament-Based Process. *Materials* **2024**, *17*, 2779. https://doi.org/10.3390/ma17112779.
17. Sadaf, M.; Bragaglia, M.; Slemenik Perše, L.; Nanni, F. Advancements in Metal Additive Manufacturing: A Comprehensive Review of Material Extrusion with Highly Filled Polymers. *J. Manuf. Mater. Process.* **2024**, *8*, 14. https://doi.org/10.3390/jmmp8010014.
18. Eickhoff, R.; Antusch, S.; Nötzel, D.; Hanemann, T. Metal fused filament fabrication (MF3) of Ti-6Al-4 V implants by using flexible, partially water-soluble binder systems. *Mater. Des.* **2025**, *254*, 114088. https://doi.org/10.1016/j.matdes.2025.114088.
19. Eickhoff, R., Nötzel, D., Oral, G., Scholz, M., Hanemann, T. Ceramic fused filament fabrication (CF3) of zirconia implants by using flexible, partially water-soluble binder systems. *Mater. Des.* **2025**, *254*, 114148. https://doi.org/10.1016/j.matdes.2025.114148.
20. Luo, J.; Gilbert, L.J.; Qu, C.; Landers, R.G.; Bristow, D.A.; Kinzel, E.C. Additive Manufacturing of Transparent Soda-Lime Glass Using a Filament-Fed Process. *J. Manuf. Sci. Eng.* **2017**, *139*, 061006. https://doi.org/10.1115/1.4035182.
21. Schilm, J.; Moritz, T.; Wagner, D.; Schwarzer, E.; Weingarten, S.; Wätzig, K. Additive Manufacturing of Functionalized Glass Components. *Ceram. Appl.* **2019**, *7*, 28–34.
22. Zhang, D.; Liu, X.; Qiu, J. 3D printing of glass by additive manufacturing techniques: A review. *Front. Optoelectron.* **2021**, *14*, 263–277. https://doi.org/10.1007/s12200-020-1009-z.
23. Kotz, F.; Arnold, K.; Bauer, W.; Schild, D.; Keller, N.; Sachsenheimer, K.; Nargang, T.M.; Richter, C.; Helmer, D.; Rapp, B.E. Three-dimensional printing of transparent fused silica glass. *Nature* **2017**, *544*, 337–339. https://doi.org/10.1038/nature22061.
24. Hambitzer, L.; Hosneolfat, Z.; Griebenow, K.; Prediger, R.; Kluck, S.; Ketterer, I.; Zaidi, S.B.; Brauer, D.S.; Kotz-Helmer, F. High-Resolution Stereolithography of Amorphous, Dense and Mechanically Stable Bioactive Glass. *Adv. Mater. Technol.* **2025**, *10*, e00925. https://doi.org/10.1002/admt.202500925.
25. Huang, K.; Franchin, G.; Nissen, D.; Erler, J.; Anaby, A.; Colombo, P. Volumetric additive manufacturing of transparent silica glass with tunable refractive index and color by xolography. *Mater. Today* **2026**, *98*, 103435. https://doi.org/10.1016/j.mattod.2026.103435.
26. Marsh, A.C.; Zhang, Y.; Poli, L.; Hammer, N.; Roch, A.; Crimp, M.; Chatzistavrou, X. 3D printed bioactive and antibacterial silicate glass-ceramic scaffold by fused filament fabrication. *Mater. Sci. Eng. C Mater. Biol. Appl.* **2021**, *118*, 111516. https://doi.org/10.1016/j.msec.2020.111516.
27. Piotter, V. A review of the current status of MicroMIM Part I. *Powder Inject. Molding Int.* **2011**, *5*, 27–36.
28. Gloeckle, C.; Konkol, T.; Jacobs, O.; Limberg, W.; Ebel, T.; Handge, U.A. Processing of Highly Filled Polymer-Metal Feedstocks for Fused Filament Fabrication and the Production of Metallic Implants. *Materials* **2020**, *13*, 4413. https://doi.org/10.3390/ma13194413.

29. Nötzel, D.; Eickhoff, R.; Pfeifer, C.; Hanemann, T. Printing of Zirconia Parts via Fused Filament Fabrication. *Materials* **2021**, *14*, 5467. https://doi.org/10.3390/ma14195467.
30. Tseng, W.J.; Liu, D.-M.; Hsu, C.-K. Influence of stearic acid on suspension structure and green microstructure of injection-molded zirconia ceramics. *Ceram. Inter.* **1999**, *25*, 191–195. https://doi.org/10.1016/S0272-8842(98)00024-8.
31. Available online: https://www.swarco-indusferica.com/en/swarcoforce (accessed on 10 September 2026).
32. Mezger, T.G. *The Rheology Handbook*, 4th ed.; Vincentz Network Publisher: Hannover, Germany, 2014. ISBN 978-3-86630-650-9.
33. German, R.M. *Sintering Theory and Practice*; John Wiley Sons, Inc.: New York, NY, USA, 1996.
34. Hambitzer, L.; Prediger, R.; Sun, Y.; Toombs, J.; Hosneolfat, Z.; Montazeri, R.; Kluck, S.; Taylor, H.K.; Kotz-Helmer, F. Computed axial lithography of multioxide glasses and ceramics from nanoparticles and organic–inorganic precursors. *Addit. Manuf. Lett.* **2025**, *15*, 100334. https://doi.org/10.1016/j.addlet.2025.100334.

Disclaimer/Publisher's Note: The statements, opinions and data contained in all publications are solely those of the individual author(s) and contributor(s) and not of MDPI and/or the editor(s). MDPI and/or the editor(s) disclaim responsibility for any injury to people or property resulting from any ideas, methods, instructions or products referred to in the content.